Numerical analysis of electrical response: Statics and dynamics of space-charge regions at blocking electrodes[a)]

Donald R. Franceschetti and J. Ross Macdonald

Department of Physics and Astronomy, University of North Carolina, Chapel Hill, North Carolina 27514
(Received 16 June 1978; accepted for publication 13 July 1978)

The steady-state and transient electrical properties of a material containing one or two species of mobile charge carrier in contact with blocking electrodes are examined. The systems treated are 2, 20, and 40 Debye lengths in extent and exemplify the transition from thin-film or membranelike behavior to the more usual case in which well-defined space-charge layers form at each electrode. The static capacitance of the electrode/material/electrode system is examined and the response of the system to a step-function applied potential difference is obtained by numerical simulation. The simulation results show clearly the role of the system length and charge carrier mobilities in determining the system response. The decay of total current following the potential step is numerically fitted to a sum of exponential decays. The nonlinear character of system response becomes apparent when the transient current associated with the formation of space-charge layers in response to a potential step is compared with that which accompanies the decay of the space-charge layers following the sudden restoration of zero potential difference between the electrodes. The redistribution of charge carriers and the electrostatic potential both in the steady state and at representative times during the transient response are presented and discussed.

PACS numbers: 66.30.Dn, 66.10.Ed, 82.45.+z

I. INTRODUCTION

The characterization of material systems by electrical response measurements requires the development of abstract models for which the response can be determined theoretically and which can serve as a basis for the reduction of experimental data. For the case of electrode/material systems in which the electrode is metallic and the material is a semiconductor or ionic conductor, the conventional model is embodied in a set of coupled nonlinear differential equations and boundary conditions which must be solved to determine the response to a given electrical perturbation. Approaches to the solution of these equations can be divided into three broad categories: small-signal treatments, physically motivated approximation schemes, and numerical solutions. A few brief comments conerning earlier work in each of these areas will provide background and motivation for the present work in which we apply numerical methods to an important but little-studied class of simple systems.

Under small-signal conditions, the system is perturbed only slightly from its equilibrium state, and the equations governing response to the perturbation can be linearized. Exact expressions have been obtained[1] for the response of electrode/material/electrode systems to small-signal ac perturbations, provided that the system is flatband (i.e., lacks intrinsic space-charge layers), contains no more than two species of mobile charge, and has bulk generation/recombination and electrode adsorption/reaction processes which meet well-defined but fairly general criteria.[2,3] To go beyond the level of present theory and to include the effects of intrinsic space-charge, or Frenkel,[4] layers and a possible dc bias on small-signal ac response will require the application of numerical methods. The present study is part of a general plan which will include treatment of these more general small-signal ac situation.

Semiconductor and electrochemical systems are frequently amenable to treatment by approximation schemes in which the material is partitioned into regions, each dominated by a single physical process. Further approximations are permissible in the case of "supported" electrolyte solutions which contain, in addition to the ions which react or are adsorbed at the electrode, an excess of indifferent electrolyte which acts to screen the bulk of the material from the applied field. There are, however, important situations in which most or all of these approximations are unjustified. For solid ionic conductors, materials with Schottky or Frenkel defects, or disordered-sublattice materials, for semiconductors, fused salts, and unsupported electrolyte solutions, the approximations made in the supported case are unjustified. For systems whose characteristic dimensions are on the order of the Debye screening length (or other length characteristic of the material), partitioning of the system is unsatisfactory. In such cases, the only reliable approach is to attempt accurate numerical solution of the full set of equations chosen to model the system. The development of accurate solutions would also appear desirable where feasible, even in cases in which the use of an approximation scheme is warranted, since new insights and possibly better approximation techniques may be suggested by the accurate and more detailed results.

[a)]Work supported by U.S. National Science Foundation (Grant NO. 76-84187).

 0021-8979/79/010291-12$01.10

A considerable literature now exists concerning the application of numerical methods to the steady-state and transient electrical response of semiconductor devices.[5-9] Another group of papers deal with the application of such techniques to electrochemical systems.[10-15] In the semiconductor literature, however, far greater attention has been given to the behavior of internal heterojunctions than to processes at the electrodes. The electrochemical literature has, for the most part, dealt with "supported"electrolyte solutions. In both the electrochemical and semiconductor cases, more attention has been given to situations in which the current through the system is controlled than those in which the applied potential drop across the system is a known function of time. Only a few papers have dealt with the transient behavior of unsupported materials in contact with blocking or partially polarizable electrodes.[10]

Both the controlled-current and the controlled-voltage cases are realized in modern experimental electrochemical methods.[16] In chronopotentiometry, the potential drop across the system resulting from an applied steady current is monitored. In chronoamperometry, the current through the system resulting from an applied potential difference is recorded, while in chronocoulometry, the charge transported through the system is determined as a function of time. In addition, a linear voltage sweep is often useful in the study of complex electrode reactions.[17] Although these methods have been primarily applied to systems with supported electrolytes, it is reasonable to assume that they would also prove useful in unsupported cases once a suitable theoretical basis is provided for their interpretation. We believe that numerical simulation of system response can play a substantial role in the establishment of that basis.

In the present work, we simulate, by numerical techniques, the response of an effectively one-dimensional electrode/material/electrode system to a near-step-function applied potential difference. It is assumed that the material contains one or two species of mobile charge carrier which are completely blocked at the electrode/material interfaces. The methods employed work well for systems of up to 50 Debye lengths in extent and can doubtless be applied to somewhat larger systems with additional effort. The range considered here is sufficient to display the transition in behavior from the limit of very thin systems, in which the applied field is only weakly screened by the mobile charge, to the more familar case in which the formation of space-charge layers near the electrode reduces the field intensity in the material interior several orders of magnitude from that originally applied. The applied potentials considered range from the small-signal limit into the nonlinear regime.

Although the final steady state of the system can be achieved by allowing the simulation to continue for a sufficiently long time, alternative treatments of the steady state are also instructive, particularly if the relationships between the position, charge density, electrostatic potential, and electric field can be expressed in closed form. One such treatment was devised by Jaffe[18] for the case of two mobile species of equal charge in the absence of immobile background charge. A second was given by Macdonald[19,20] for the case of a single mobile charge species with compensating background charge. Both treatments involve parameters which must be determined to satisfy self-consistency criteria. Efficient computer programs for this determination have also been developed in the present work.

For clarity, this paper is divided into sections. In Sec. II, the basic equations of the assumed model are presented and a system of normalized units chosen. The steady-state problem is discussed in Sec. III. Computational aspects of the time-dependent problem are discussed in Sec. IV, and the results of our numerical simulations are presented in Sec. V. Section VI is a brief summary.

II. GENERAL EQUATIONS

We consider a homogeneous slab of material, a single crystal or homogeneous solution, of length l, extending between two identical plane-parallel electrodes. The material is assumed to contain a single species of positive mobile charge carrier and a single species of negative mobile charge carrier. The concentrations of these species will be denoted $p(x)$ and $n(x)$, respectively, and their charges taken to be $z_p e$ and $-z_n e$, where e is the proton charge. The flux densities of the two charge species are assumed to be given by the Nernst-Planck equations:

$$J_p = \mu_p p E - D_p \frac{\partial p}{\partial x} \tag{1}$$

and

$$J_n = -\mu_n n E - D_n \frac{\partial n}{\partial z} \tag{2}$$

where μ_p and μ_n are the mobilities of the charges, D_p and D_n are their diffusion coefficients, and E is the electric field. E is related to the electrostatic potential gradient in the usual way, $E \equiv -(\partial V/\partial x)$, and E and V obey the macroscopic Poisson equation

$$\frac{\partial E}{\partial x} = -\frac{\partial^2 V}{\partial x^2} = \frac{4\pi e}{\epsilon}(z_p p - z_n n + \rho_0), \tag{3}$$

where ϵ is the dielectric constant of the material and ρ_0 is the density of immobile background charge, if any is present. The boundary conditions appropriate to blocking electrodes are

$$J_p(x=0) = J_n(x=0) = 0 \tag{4}$$

and

$$J_p(x=l) = J_n(x=l) = 0. \tag{5}$$

The time evolution of the system is determined by the equations of continuity

$$\frac{\partial p}{\partial t} = -\frac{\partial J_p}{\partial x} \tag{6}$$

and

$$\frac{\partial n}{\partial t} = -\frac{\partial J_n}{\partial x}. \tag{7}$$

In the present work, we do not allow for the generation and

recombination of the charged species; such processes will be considered in future work. The total current I is the sum of Faradaic components and the displacement current,

$$I=z_p eJ_p-z_n eJ_n-\frac{\epsilon}{4\pi}\frac{\partial^2 V}{\partial t\,\partial x}. \tag{8}$$

In a one-dimensional system, I is spatially constant.[21]

It is assumed throughout this work that the charge mobilities and diffusion coefficients are field and concentration independent and that the diffusion coefficients are related to the mobilities through the familiar Einstein relations

$$D_p=\mu_p k_B\theta/z_p e, \quad D_n=\mu_n k_B\theta/z_n e, \tag{9}$$

where k_B is Boltzmann's constant and θ is the absolute temperature. These assumptions, together with the use of the macroscopic electrostatic potential and field in Eqs. (1)–(3), are idealizations of the physical system which are frequently made in modelling the electrical response of materials. The reliability of the resulting model may vary from one material and set of conditions to another.

For maximum generality and conciseness, a set of normalized dimensionless quantities will be employed.[22] We will require the charge and mobility ratios

$$\pi_z\equiv z_n/z_p, \quad \pi_m\equiv\mu_n/\mu_p, \tag{10}$$

and the related ratios

$$\pi_e\equiv\pi_m(n_e/p_e), \quad \pi_f\equiv\pi_z(n_e/p_e), \tag{11}$$

where p_e and n_e are the equilibrium concentrations of the mobile charges. These permit the definition of the further useful quantities

$$\epsilon_p\equiv(1+\pi_e)^{-1}, \quad \epsilon_n\equiv(1+\pi_e^{-1})^{-1}, \tag{12}$$

$$\delta_p\equiv(1+\pi_f)^{-1}, \quad \delta_n\equiv(1+\pi_f^{-1})^{-1}, \tag{13}$$

and

$$\lambda_p\equiv\delta_p/\epsilon_p, \quad \lambda_n\equiv\delta_n/\epsilon_n. \tag{14}$$

The variables of the problem are normalized with respect to the Debye length

$$L_D\equiv[\epsilon k_B\theta/4\pi e^2(z_n^2 n_e+z_p^2 p_e)]^{1/2}, \tag{15}$$

the conductivity

$$\sigma\equiv e(z_p p_e\mu_e+z_n n_e\mu_n), \tag{16}$$

and the dielectric relaxation time

$$\tau\equiv\epsilon/4\pi\sigma \tag{17}$$

as follows:

$$X\equiv x/L_D, \tag{18}$$

$$T\equiv t/\tau_D, \tag{19}$$

$$J_p^*\equiv z_p e^2 L_D J_p(1+\pi_z\pi_e)/\sigma k_B\theta, \tag{20}$$

$$J_n^*\equiv z_n e^2 L_D J_n(1+\pi_z^{-1}\pi_e^{-1})/\sigma k_B\theta, \tag{21}$$

$$I^*\equiv eL_D I/\sigma k_B\theta, \tag{22}$$

$$V^*\equiv eV/k_B\theta, \tag{23}$$

$$E^*\equiv eEL_D/k_B\theta. \tag{24}$$

Further, the concentrations of the charged species have the normalized forms

$$P\equiv p/z_p p_e, \tag{25}$$

$$N\equiv n/z_n n_e, \tag{26}$$

and

$$\nu\equiv\rho_0/(z_n^2 n_e+z_p^2 p_e). \tag{27}$$

In terms of the normalized variables, the basic equations (1)–(3) and (6)–(8) take the forms

$$J_p^*=-z_p PV^{*\prime}-P', \tag{28}$$

$$J_n^*=z_n NV^{*\prime}-N', \tag{29}$$

$$V^{*\prime\prime}=\delta_n N-\delta_p P-\nu, \tag{30}$$

$$\lambda_p\dot{P}=-J_p^{*\prime}, \tag{31}$$

$$\lambda_n\dot{N}=-J_n^{*\prime}, \tag{32}$$

and

$$I^*=\epsilon_p J_p^*-\epsilon_n J_n^*-\dot{V}^{*\prime}, \tag{33}$$

where a dot over a quantity indicates partial differentiation with respect to T and a prime indicates partial differentiation with respect to X.

It is convenient also to introduct the normalized half-length of the system,

$$M\equiv l/2L_D. \tag{34}$$

It will be assumed below that in normalized units the system extends from $X=-M$ to $X=M$.

For systems in which only one species in mobile, the more natural unit of length is

$$L_{D_1}\equiv(\epsilon k_B\theta/4\pi e^2 z_m^2 c_m)^{1/2}, \tag{35}$$

where z_m and c_m are the charge and concentration, respectively, of the single mobile species. The corresponding normalized half-length is

$$M_1=l/2L_{D_1}. \tag{36}$$

In the present work, however, the normalized half-length of the material will be expressed in terms of M, rather than M_1, to facilitate comparisons with the two-mobile case.

The results presented here are obtained for $z_n=z_p=1$ and $\nu=0$. It is a simple matter to scale the solutions so that they apply in the case $z_n=z_p\equiv z_e\geqslant 1$. Let $\{P,N,V^*,J_p^*,J_n^*,I^*\}$ denote the solutions for $z_e=1$, given values of M, π_m, and ν, and a given applied normalized potential difference $V_a^*(T)$. It can then readily be shown that $\{P/z_e, N/z_e, V^*/z_e, J_p^*/z_e, J_n^*/z_e, I^*/z_e\}$ is the solution for the same values of M and π_m and $z_e>1$ when the normalized background charge is ν/z_e and the normalized applied potential difference is V_a^*/z_e.

III. STEADY STATE

The steady-state conditions are given by Eqs. (28)–(30), with $J_p^*=J_n^*=0$. Since no current flows, the steady state is one of thermal equilibrium. An exact treatment of the steady state was given by Jaffé[18] for two mobile charge species which undergo generation and recombination so that the product PN remains equal to unity. Jaffé also indicated how the case of zero generation/recombination (G/R) might be treated but did not present the solution in detail. On extending the approach indicated by Jaffé, we obtain the following results for two mobile charge species, blocking electrodes, and zero G/R.

Let the potentials of the left-hand and right-hand electrodes be $\frac{1}{2}V_a^*$ and $-\frac{1}{2}V_a^*$, respectively. Further, let E_0^* denote the value of E^*, and C_0 the common value of P and N at the center of the system in the steady state. The solution has two forms, one for $E_0^*\leqslant 2C_0^{1/2}$ and one for $E_0^*\geqslant 2C_0^{1/2}$.

In the low-field case, $E_0^*\leqslant 2C_0^{1/2}$, the potential and field are given by

$$V^*=\ln\left(\frac{\mathrm{dn}(XC_0^{1/2},\kappa)-(1-\kappa^2)^{1/2}\,\mathrm{sn}(XC_0^{1/2},\kappa)}{\mathrm{dn}(XC_0^{1/2},\kappa)+(1-\kappa^2)^{1/2}\,\mathrm{sn}(XC_0^{1/2},\kappa)}\right) \tag{37}$$

and

$$E^*=\frac{[4C_0(1-\kappa^2)]^{1/2}}{\mathrm{cn}(XC_0^{1/2},\kappa)}, \tag{38}$$

where sn, cn, and dn are Jacobian elliptic functions.[23] The charge concentrations are then given by the Boltzmann relations

$$P=C_0\exp(-V^*) \tag{39}$$

and

$$N=C_0\exp(V^*). \tag{40}$$

The solutions contain two quantities, the concentration C_0 and the modulus κ, which must be chosen in the present case of zero G/R so that the total number of particles of each species is conserved and the electrostatic potential has the correct value at the electrodes. The former condition may be stated as

$$\int_{-M}^{M}P\,dX=\int_{-M}^{M}N\,dX=2M, \tag{41}$$

and the latter condition can be simplified to

$$(1-\kappa^2)^{1/2}=\frac{\mathrm{cn}(MC_0^{1/2},\kappa)}{\mathrm{sn}(MC_0^{1/2},\kappa)}\sinh\left(\frac{V_0^*}{4}\right). \tag{42}$$

In the high-field case $E_0^*\geqslant 2C_0^{1/2}$, the potential and field are given by

$$V^*=\ln\left(\frac{1+\mathrm{sn}(\frac{1}{2}XQ,\kappa)}{1-\mathrm{sn}(\frac{1}{2}XQ,\kappa)}\right) \tag{43}$$

and

$$E^*=Q\,\frac{\mathrm{dn}(\frac{1}{2}XQ,\kappa)}{\mathrm{cn}(\frac{1}{2}XQ,\kappa)}, \tag{44}$$

where

$$Q\equiv[4C_0/(1-\kappa^2)]^{1/2}. \tag{45}$$

The concentrations are given as in Eqs. (39) and (40), and as in the previous case, C_0 and κ are determined by the requirements that particles be conserved and that the potential at the electrodes have the specified values.

An efficient numerical algorithm was written to evaluate C_0 and κ. First, estimates of these quantities are made. Then, for the chosen value of C_0, a value of κ satisfying Eq. (42), or the equivalent high-field condition, to specified accuracy, is formed by Newton-Raphson iteration. Using C_0 and the new value of κ, the quantity

$$S\equiv C_0^{-1}\int_{-M}^{M}P\,dX \tag{46}$$

is evaluated and an average of C_0 and $2M/S$ is used as a new estimate of C_0. The procedure is then repeated until satisfactory convergence of both C_0 and κ is attained. The Jacobian elliptic functions are computed using the algorithms of Hofsommer and van de Riet,[24] and the numerical integration is accomplished using a double-precision version of QUAD, a robust procedure for numerical quadrature, written by Blue[25] and contained in the PORT subroutine library.[26]

In an earlier paper, one of us (J.R.M.) examined the Jaffé solution in some detail.[27] The treatment presented in that paper was stated, incorrectly, to apply when G/R did not occur. The expressions obtained in that work are, however, applicable in Jaffé's original case[18] in which G/R processes ensure that the product NP retains its equilibrium value of unity and do apply in the limit $V_a^*\ll M$ of the present case for which $NP\approx 1$.

An exact treatment of the steady state for a single mobile species, possibly subject to bimolecular G/R with the fixed charge species, was given by Macdonald.[19,20] It is summarized here for the case of zero G/R and the negative species mobile. For a given value of V_a^*, one first determines

$$V_d^*\equiv V_a^*-\ln\{V_a^*/[1-\exp(-V_a^*)]\} \tag{47}$$

and sets the potential of the left-hand electrode as $V_a^*-V_d^*$ and the potential of the right-hand electrode as $-V_d^*$. The concentration of mobile carriers is then given by

$$N=\exp(V^*), \tag{48}$$

and the electric field is given by

$$E^*=[c_0+\exp(V^*)-1-V^*]^{1/2}, \tag{49}$$

where c_0 is a constant chosen so that

$$2M=\int_{-V_d^*}^{V_a^*-V_d^*}\frac{dV^*}{E^*(V^*)}. \tag{50}$$

Once c_0 is determined, it is a simple matter to evaluate n, E^*, and

$$X=\int_{V^*}^{V_a^*-V_d^*}\frac{dV^*}{E^*(V^*)}-M \tag{51}$$

for any value of V^* between $-V_d^*$ and $V_a^*-V_d^*$. A program was written to evaluate c_0 by a Newton-Raphson method applied to the difference between M and the corresponding integral [Eq. (50)] evaluated using QUAD, as in the previous case.

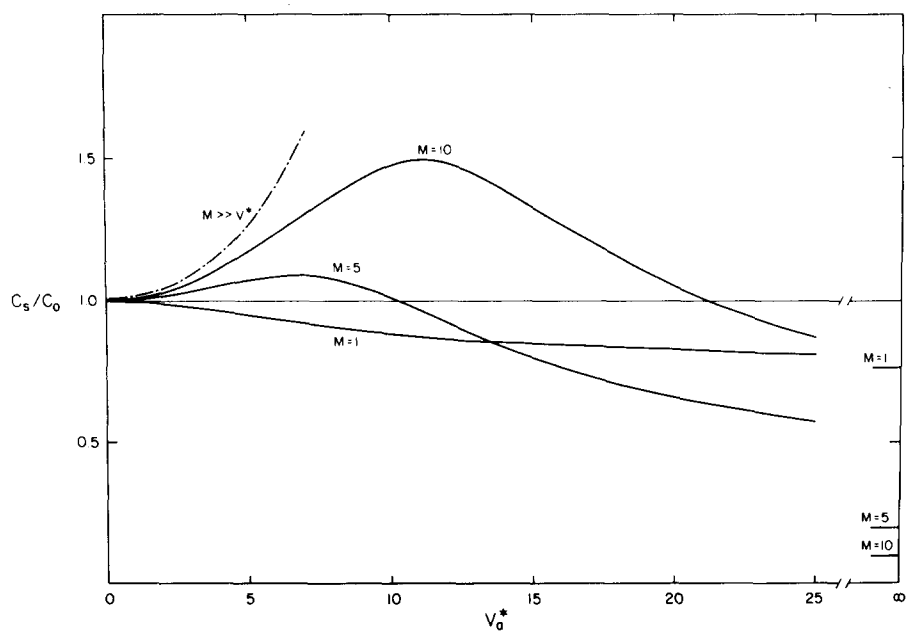

FIG. 1. Static capacitance as a function of applied potential drop for systems with two-mobile charge carrier species.

The distributions of charge carrier concentration and the electrostatic potential in the steady state will be considered in Sec. V, where they will be compared with dynamic response results. Further steady-state quantities of interest are the total static capacitance of the system, $C_s \equiv q/V_a$, and the differential capacitance $C_d \equiv dq/dV_a$, where q is the charge on the positive electrode and V_a is the (unnormalized) applied potential difference. The static capacitance may be written as

$$C_s = 2ME_0^* C_g / V_a^*, \tag{52}$$

where E_0^* is the value of the normalized field at the electrode and $C_g \equiv \epsilon/4\pi l$ is the geometric capacitance of the system. The differential capacitance is given by

$$C_d = 2MC_g \frac{dE_0^*}{dV_a^*} = C_s + V_a^* \frac{dC_s}{dV_a^*}. \tag{53}$$

The static capacitance for the two-mobile case is shown in Fig. 1 for $M=1$, 5, and 10. The capacitance at $V_a^*=0$ is given by[27]

$$C_0 = C_g M \operatorname{ctnh}(M), \tag{54}$$

and the static capacitance must approach C_g as $|V^*| \to \infty$. Also shown in Fig. 1 is the limiting capacitance for $M \gg V$, given by[27]

$$C_s/C_0 = \frac{\sinh(\frac{1}{4}V_a^*)}{\frac{1}{4}V_a^*}, \tag{55}$$

which is the prediction of the Jaffé theory for the case in which $NP=1$ is preserved by G/R. It was found that beyound the maximum in C_s, as C_s approaches C_g, the quantity $C_s - C_g$ appeared to vanish as $(V_a^*)^{-1}$. The qualitative behavior of the differential capacitance can be inferred from Fig. 1 and Eq. (53). C_d also approaches C_g as V_a^* becomes large, and the quantity $C_d - C_g$ was found to vanish more rapidly than $(V_a^*)^{-1}$.

The static capacitance for the one-mobile case is shown in Fig. 2 for $M=1$, 5, and 10. The capacitance at $V_a^*=0$ is given by[20]

$$C_0 = C_g M_1 \operatorname{ctnh}(M_1) = C_g(M/\sqrt{2}) \operatorname{ctnh}(M/\sqrt{2}). \tag{56}$$

In the one-mobile case, also, it was found that as C_s and C_d approached the limiting value C_g the difference $C_s - C_g$ vanished as $1/V_a^*$ and the difference $C_d - C_g$ vanished more rapidly. Before this limiting behavior is attained, however, the one-mobile and two-mobile cases are qualitatively different. In the two-mobile case, C_s increases to a maximum, while in the one-mobile case, C_s decreases monotonically. It is reasonable that such a difference in behavior be observed since a single mobile species is less able to screen the electric field than are two-mobile species of opposite signs.

IV. NUMERICAL SIMULATION TECHNIQUES

The time evolution of the electrode/material/electrode system is governed by Eqs. (28)–(32) together with the appropriate boundary conditions on J_p^*, J_n^*, and V^* at the electrodes. On defining $U_1 \equiv P$, $U_2 \equiv N$, and $U_3 \equiv V^*$, and com-

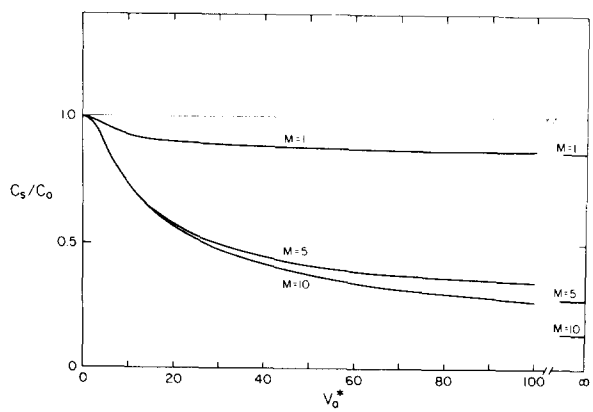

FIG. 2. Static capacitance as a function of applied potential drop for systems with one mobile charge carrier species.

bining equations to eliminate J_p^* and J_n^*, we obtain three partial differential equations of the general form

$$A_i \frac{\partial U_i}{\partial T} = f_i\left(X, U_j, \frac{\partial U_j}{\partial X}, \frac{\partial^2 U_j}{\partial X^2}\right) \tag{57}$$

and six boundary conditions of the form

$$\left[b_i\left(T, U_j, \frac{\partial U_j}{\partial X}\right)\right]_{X=\pm M} = 0. \tag{58}$$

It is assumed that at $T=0$ the system is in equilibrium with $P=N=1$ and $V^*=0$ throughout.

The approach most commonly chosen in previous work on related problems is the finite-difference method[28,29] in which the continuous variables X and T are replaced by a lattice of points (X_n, T_m) at which the values of the approximate solution U_{in}^m are calculated. In most such work, the general equation (57) is approximated by

$$\begin{aligned} A_i\left(\frac{U_{in}^{m+1}-U_{in}^m}{T_{m+1}-T_m}\right) &= f(X_n, \beta U_{jn}^{m+1}+(1-\beta)U_{jn}^m, \\ &\quad \beta(\Delta_1 U_j)_n^{m+1}+(1-\beta)(\Delta_1 U_j)_n^m, \\ &\quad \beta(\Delta_2 U_j)_n^{m+1}+(1-\beta)(\Delta_2 U_j)_n^m), \end{aligned} \tag{59}$$

where $(\Delta_1 U_j)_n^m$ and $(\Delta_2 U_j)_n^m$ are finite-difference approximations to the first and second spatial derivatives of U_j at the lattice point (X_n, T_m) and β is a number satisfying $0 \leqslant \beta \leqslant 1$. An analogous approximation is made for the boundary conditions (58). If the spatial coordinates are chosen to occur at uniform intervals (uniform spatial mesh) with $X_{n+1}-X_n \equiv \Delta X$, one may set

$$(\Delta_1 U_j)_n^m \equiv (U_{jn+1}^m - U_{jn-1}^m)(2\Delta X)^{-1} \tag{60}$$

and

$$(\Delta_2 U_j)_n^m = (U_{jn+1}^m - 2U_{jn}^m + U_{jn-1}^m)(\Delta X)^{-2}. \tag{61}$$

The differential equations (57) and boundary conditions (58) are thereby reduced to a set of simultaneous algebraic equations which are readily solved for each successive time interval of the lattice.

The discretization error inherent in the finite-difference method may be estimated in a number of ways. A very general analysis[28] based on a Taylor-series expansion of the U_i about the lattice points shows that for a uniform spatial mesh the error in the step from $T=T_m$ to $T=T_{m+1}$ is the sum of a term proportional to ΔT and a term proportional to $(\Delta X)^2$. Since the quantities P, N, and V^* will in general vary quite rapidly near the electrodes, application of the procedure described above, with a uniform spatial mesh, would require an enormous number of spatial intervals (>100 in many of the cases considered). The basic procedure can, however, be modified to permit the use of a far smaller number of spatial mesh points while retaining an acceptible level of overall accuracy. A logical modification would be to use more accurate finite-difference analogues of the spatial derivatives. This procedure, unfortunately, leads to more complex algebraic equations. An alternative modification which can be most effective is the use of a nonuniform spatial mesh with appropriate finite-difference analogues for the spatial derivatives. In the case of a nonuniform spatial mesh, the Taylor-series error estimate depends on the lengths of the mesh intervals through a term of the form[30,31]

$$\sum_n c_n (X_{n+1}-X_n). \tag{62}$$

The constants c_n depend on the spatial derivatives of the solutions being approximated and will be smallest when the solution varies only slightly for $X_n < X < X_{n+1}$. A systematic procedure for optimizing a nonuniform spatial mesh has been given by McAfee.[30,31] Although implementation of McAfee's procedure in the case of several coupled equations in itself would require considerable computation, the reasoning underlying his analysis, which has been indicated above, allows one to select an acceptable nonuniform mesh if the qualitative characteristics of the solution are known. Previous work on related problems using nonuniform spatial meshes includes that of DeMari[7] and Brumleve and Buck.[15]

The parameter β in Eq. (59) is important in determining the stability and accuracy of finite-differences schemes.[28] With $\beta=0$, the procedure is termed explicit, since U_{in}^{m+1} depends only on the solution at $T=T_m$ and not (implicitly) on other components of the solution at $T=T_{m+1}$. Although the finite-difference equations are easiest to solve in the explicit case, stability considerations serverely limit the maximum size of time interval usable in the procedure. In contrast, the fully implicit method, with $\beta=1$, is unconditionally stable, allowing greater freedom in the selection of time and spatial intervals. The Crank-Nicolson method,[28] with $\beta=0.5$, offers, in principle, smaller discretization errors than the fully explicit or implicit methods.

Finite-element methods[29,32] offer an alternative to finite-difference methods. In the finite-element approach, the solution is found as a linear combination of localized functions with coefficients determined by minimization of one or more integrals which arise either from a variational[33] formulation of the problem or an error estimation procedure. The finite-element solution is defined with respect to a lattice of space-time points, as in the finite-difference case, and in simpler cases is taken to be linear between the mesh points.

Our computer simulations of system response were executed with the aid of POST, a package of FORTRAN subroutines written by Schryer[34] for the solution of partial and ordinary differential equations in space and time. In the POST procedure, the time derivatives appearing in the equations are replaced by finite-difference expressions as in Eq. (57), but the spatial derivatives are retained. The resulting set of ordinary differential equations in space relate the solution at $T=T_{m+1}$ to that found at $T=T_m$. These equations are solved by an iterative procedure in which the equations are linearized and the resulting linear equations are solved by Galerkin's method applied to a basis of B splines, a sophisticated procedure related to the finite-element method.

In order to use Galerkin's method and the POST program, the PDE's must first be placed in divergence form. Equations (28)–(32) thus become

$$\lambda_p \frac{\partial P}{\partial T} = \frac{\partial}{\partial X}\left(\frac{\partial P}{\partial X} + P\frac{\partial V^*}{\partial X}\right), \tag{63}$$

$$\lambda_n \frac{\partial N}{\partial T} = \frac{\partial}{\partial X}\left(\frac{\partial N}{\partial X} - N\frac{\partial V^*}{\partial X}\right), \tag{64}$$

and

$$\delta_n N - \delta_p P = \frac{\partial}{\partial X}\left(\frac{\partial V^*}{\partial X}\right), \tag{65}$$

all of which are of the form

$$A_i\left(U_j, \frac{\partial U_j}{\partial T}\right) = \frac{\partial}{\partial X} f_i\left(U_j, \frac{\partial U_j}{\partial X}\right). \tag{66}$$

After discretization in time, Eq. (66) becomes

$$A_i\left(\beta U_j^{m+1} + (1-\beta)U_j^m, \frac{U_j^{m+1} - U_j^m}{T_{m+1} - T_m}\right)$$

$$= \frac{\partial}{\partial X} f_i(\beta U_j^{m+1} + (1-\beta)U_j^m,$$

$$\beta\frac{\partial U_j^{m+1}}{\partial X} + (1-\beta)\frac{\partial U_j^m}{\partial X}\Big), \tag{67}$$

where U_j^m is the approximate solution at $T = T_m$. We have found a fully implicit procedure, with $\beta = 1$, to be quite satisfactory. The equations of the form of Eq. (67) are then solved subject to the appropriate boundary conditions using an iterative procedure[34] in which linearized equations are formed and solved by Galerkin's method.[34,35] The basis set of B splines in which U_{jm+1} is ultimately expressed is specified by a spatial mesh of N_Δ points, $X_1 < X_2 < \ldots < X_{N_\Delta}$, and an integer k, the order of the B spline. (In the formal theory of B splines,[35,36] the endpoints of the mesh are considered to be k-fold degenerate.) There are $(N_\Delta + 2k - 2)$ basis functions which are polynomials of degree $< k$ on each mesh interval (X_n, X_{n+1}) and are continuous up to the $(k-2)$ derivative at the interior mesh points.[35,36] We found $k = 4$ to be adequate for our work.

The flexibility of the set of B-spline basis functions of order 4 permits the use of a far smaller number of spatial mesh points than would be required in a finite-difference calculation. We found it convenient and economical to use a symmetrical mesh in which the first spatial interval, $\Delta X_1 \equiv X_2 - X_1$, was quite small and each subsequent interval was $\exp(\Lambda)$ times the length of the preceding interval, up to the center of the system. The optimum values of Λ and N_Δ depend on M and V_a^*. Consideration of the conditioning of the Galerkin method limits the magnitude of Λ which can be used[37]; however, Λ's up to ln2 are generally acceptible in double-precision (~ 14 significant figure) calculations and allow considerable flexibility in the choice of the spatial mesh. The length of the nth and $(N_\Delta - n)$th spatial intervals is given by

$$\Delta X_n = \frac{M\exp(n\Lambda - \Lambda)[\exp(\Lambda) - 1]}{2\{\exp[\frac{1}{2}(N_\Delta - 1)\Lambda] - 1\}}. \tag{68}$$

Representative values of N_Δ and Λ are given in Table I.

TABLE I. Representative values of spatial mesh parameters N_Δ and Λ [Eq. (58)] and total CPU excution time for simulations of transient response ($\pi_m = 1$).

M	V_a^*	N_Δ	Λ	CPU time (sec)
1	0.01	10	0.	75
1	5	19	0.35	283
10	0.01	19	0.30	164
10	5	27	0.45	455

The equations actually employed in our calculations include, in addition to Eqs. (53)–(55) and the blocking boundary conditions

$$\left[\frac{\partial P}{\partial X} + P\frac{\partial V^*}{\partial X}\right]_{X=\pm M} = 0 \tag{69}$$

and

$$\left(\frac{\partial N}{\partial X} - N\frac{\partial V^*}{\partial X}\right)_{X=\pm M} = 0, \tag{70}$$

boundary conditions on V^* and several ordinary differential equations (ODE's). The boundary conditions on V^* were $V^*(M) = 0$ and $V^*(-M) = V_{dr}^*(T)$, where

$$V_{dr}^* = 2\times 10^4 V_a^* T, \quad 0 \leqslant T < 5\times 10^{-5}$$

$$= V_a^*, \quad 5\times 10^{-5} \leqslant T. \tag{71}$$

The computed response should differ very little after $T \approx 10^{-3}$ from that for a pure step function. It was decided not to use a pure step function (for which the total current is singular at $T = 0$) so that the total current could be determined simultaneously with the solution of the PDE's.

The POST program provides a capability for solving, simultaneously with the PDE's, a set of ODE's or algebraic equations in time which are coupled to the PDE's at fixed points in space. Using this feature, we were able to determine the total current

$$I^* = -\epsilon_p P\frac{\partial V^*}{\partial X} - \epsilon_p\frac{\partial P}{\partial X} - \epsilon_n N\frac{\partial V^*}{\partial X}$$

$$+\epsilon_n\frac{\partial N}{\partial X} - \frac{\partial^2 V^*}{\partial X\,\partial T} \tag{72}$$

for all times at arbitrary points in the system. The degree of constancy of the total current throughout the system provides an important check on the accuracy of the calculation. A second equation

$$I^* = \frac{dQ}{dT} \tag{73}$$

was included at one of the points to permit direct determination of the net (normalized) charge Q on the electrodes as the system evolves.

The coupling of ODE's to the PDE's of the system also makes it possible, in principle, to consider driving potentials applied to a circuit in which the electrode/material/electrode system is placed in series or parallel with other elements whose I-V characteristics are known. This feature may prove useful in treating systems with $M \gg V_a^*$, in which the central or bulk region behaves approximately as a parallel RC section in series with the electrode regions. In such a case, we consider a smaller system with M of the order of $2V_a^*$ in series with the RC section. We suppose the section to be connected at the left-hand electrode and let V_{RC}^* denote the potential drop across the RC elements. Then the former condition on $V^*(-M)$ is replaced by

$$V^*(-M)=V_{dr}^*(T)-V_{RC}^* \tag{74}$$

and the ODE

$$I=\frac{V_{dr}^*(T)-V_{RC}^*}{R}+C\frac{d\,[V_{dr}^*(T)-V_{RC}^*]}{dT} \tag{75}$$

is added to the set of equations.

The POST program provides for automatic selection of time step size, consistent with error limits set by the user. The limits apply to the error in the B-spline representation of the solution with respect to the optimum B-spline representation for the assumed spatial mesh. Thus, the adequacy of the spatial mesh and B-spline order chosen must be verified by the user. Fortunately, numerous criteria exist to determine whether the error limits and B-spline basis chosen for a particular simulation are in fact adequate. Aside from the obvious procedure of repeating the simulation with smaller error limits and a finer spatial mesh, one may verify that the total current remains spatially constant throughout the simulation and that the resulting steady state agrees with the results of the exact treatment discussed in Sec. III. Further, for the special case in which the mobility ratio π_m is unity, the symmetry of the system guarantees that $P(X)=N(-X)$ and $V^*(X)=V_a^*-V^*(-X)$. Finally, one may, and should, verify that the total quantity of each species of charge remains constant throughout the simulation.

The error limits chosen were 3×10^{-3} for the relative error and 10^{-6} for the absolute error. The POST program is designed so that the maximum error in P, N, and V^* at each step would then be 3×10^{-3} times the maximum absolute value of the quantity, plus the absolute error, and the maximum error in I^* and Q at each step would be 3×10^{-3} times the absolute value of the quantity, plus the absolute error. We have found, however, that with an adequate spatial mesh the solution is far more accurate, when tested as described above, than these limits would indicate. We estimate that the results given in Sec. V, which required 50 or more time steps in some cases, are accurate to within about 1% throughout.

No discussion of numerical simulation is complete without some discussion of the computer time required. Some representative times for an IBM 370/155 computer are included in Table I. Despite the high efficiency of the POST program, computational expense limited the total number of simulations which we could perform at the desired level of accuracy.

V. TRANSIENT RESPONSE

Simulations were executed for systems of lengths $M=1$ and 10, for applied potentials ranging from $V_a^*=0.01$ to 10, and for three values of the mobility ratio $\pi_m=1$, 5, and ∞. Two additional simulations with $M=20$ are discussed below. The time dependence of the total current is shown in Figs. 3–5. In these plots, I^* is expressed in units of $I_0^*\equiv V_a^*/2M$, the current which flows immediately after the potential is applied. The time after application of the potential step is expressed in units of M, which permits plotting the response for different M's in the same figure.

Figure 3 displays the current-vs-time behavior for systems in which $\pi_m=1$. For $M=1$, it is seen that the decrease of the current occurs most rapidly for $V_a^*=10$ and least rapidly for $V_a^*=0.01$. In contrast, for $M=10$, the most rapid current decrease occurs for the smallest applied potential. This behavior is consistent with, and required by, the results obtained in the steady-state treatment of Sec. III. As Fig. 1 shows, for $M=1$, the capacitance of the system decreases as V_a^* increases (except for $V_a^*\ll1$). Thus, a proportionately smaller charge must build up on the electrodes for $V_a^*=5$ than for $V_a^*=0.01$ and smaller for $V_a^*=10$ than for $V_a^*=5$. In

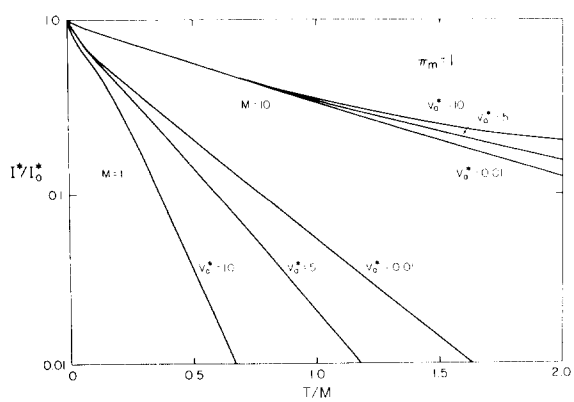

FIG. 3. Current-time curves for transient response of systems with a mobility ratio π_m of unity.

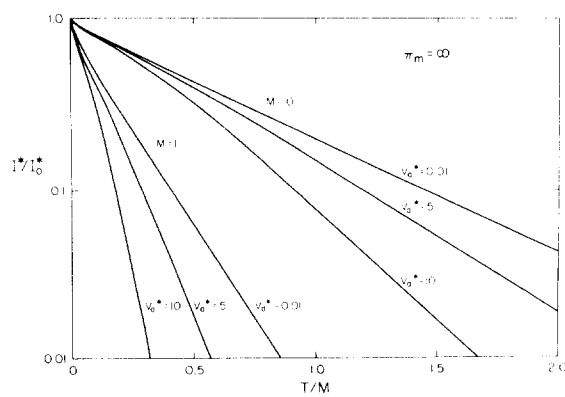

FIG. 4. Current-time curves for transient responses of systems with a mobility ratio π_m of infinity (only negative carriers mobile).

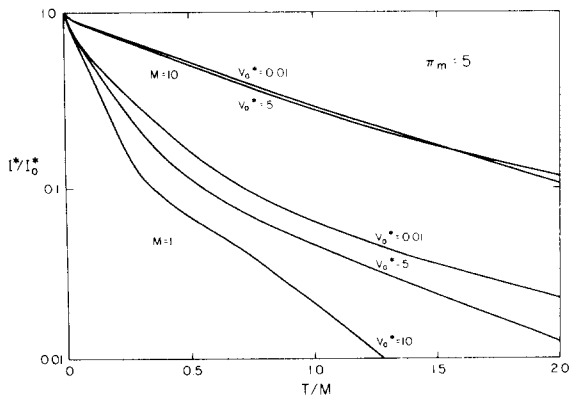

FIG. 5. Current-time curves for transient response of systems with a mobility ratio $\pi_m = 5$.

the $M = 10$ case, the capacitance increases as V_a^* increases until $V_a^* \approx 11$ is reached. Thus, in this case, a proportionately larger charge must flow onto the electrodes for $V_a^* = 5$ than for $V_a^* = 0.01$ and larger for $V_a^* = 10$ than for $V_a^* = 5$.

In Fig. 4, the current-vs-time behavior is given for systems in which $\pi_m = \infty$ so that only negative charge carriers are mobile. In this case, for both $M = 1$ and 10, the decrease in current occurs increasingly rapidly with increasing V_a^*. This behavior is also consistent with the results obtained for the steady-state one-mobile case since, as Fig. 2 shows, the capacitance of the system decreases monotonically with increasing V_a^*.

The $\pi_m = 5$ case shown in Fig. 5 is intermediate between the $\pi_m = 1$ and $\pi_m = \infty$ cases and can be understood qualitatively in terms of the other two cases. Since the more mobile charge species will respond to a suddenly applied electric field more rapidly than the less mobile species, the system response occurs in two stages. In the first stage, its behavior resembles that of a one-mobile system. In the second, the less mobile charges complete their response to the now screened electric field, while the more mobile charges readjust from their one-mobile quasi-steady-state distribution to the two-mobile steady-state distribution. A clear break in slope is visible in the $M = 1$ curves, while the $V_a^* = 5$ and $= 0.01$ curves actually cross in the $M = 10$ case, showing a transition from one-mobile to two-mobile behavior.

The current-vs-time curves were fitted to a sum of exponential decays

$$I^*/I_0^* = \sum_{i=1}^{N_t} c_i \exp(-\alpha_i T/M), \tag{76}$$

using the program of Provencher[38,39] which employs a Four-

TABLE II. Coefficients, exponents, and standard deviation of exponential fits [Eq. (66)] to current-time curves (Figs. 3–5).

System (M,π_m)	V_a^*	c_1	α_1	c_2	α_2	c_3	α_3	c_4	α_4	σ
(1,1)	0.01	0.8311	2.722	0.1119	34.60	0.0373	433.8	...	...	2.3×10^{-3}
	1.	0.8323	2.726	0.1174	38.11	0.0389	575.1	...	...	1.8×10^{-3}
	2.	0.8408	2.840	0.1058	39.03	0.0413	467.7	...	...	1.1×10^{-3}
	3.	0.8572	3.048	0.0970	51.25	0.0350	636.7	...	...	1.2×10^{-3}
	5.	0.8875	3.588	0.0811	94.26	0.0267	1405.	...	...	3.1×10^{-2}
	10.	0.9402	5.396	0.0532	546.0	...	...	...	...	1.5×10^{-2}
(10,1)	0.01	0.9552	1.067	0.0301	37.23	0.0121	762.4	...	...	1.6×10^{-3}
	1.	0.9466	1.049	0.0176	10.23	0.0245	68.86	0.0098	1271	5.5×10^{-4}
	3.	0.3679	0.6945	0.5889	1.347	0.0302	49.20	0.0116	1001	5.9×10^{-4}
	5.	0.2874	0.4690	0.6726	1.412	0.0029	63.64	0.0104	1298	6.0×10^{-4}
	10.	0.2567	0.2463	0.7077	1.550	0.0026	90.60	0.0086	1883	6.5×10^{-4}
(20,1)	0.01	0.9617	0.9620	0.0318	10.93	...	...	...	...	2.7×10^{-3}
	5	0.2698	0.4048	0.7097	1.317	0.0184	163.8	...	...	1.2×10^{-3}
(1,5)	0.01	0.1340	0.8915	0.7080	4.430	0.1101	58.31	0.0387	940.3	1.8×10^{-3}
	1.	0.1335	0.8977	0.7111	4.495	0.1071	59.17	0.0415	859.6	1.4×10^{-3}
	3.	0.1327	0.9745	0.7347	5.036	0.0912	82.36	0.0353	1124.	5.2×10^{-4}
	5.	0.1233	1.098	0.7704	5.845	0.0751	139.6	0.0264	1864.	1.9×10^{-3}
	10.	0.0987	1.577	0.8376	8.241	0.0562	613.6	...	...	5.3×10^{-2}
(10,5)	0.01	0.0460	0.2446	0.8986	1.261	0.0490	56.06	...	...	2.9×10^{-3}
	1.	0.5820	0.9112	0.3650	1.823	0.0364	42.52	0.0145	781.7	7.6×10^{-4}
	5.	0.0738	0.05914	0.8785	1.421	0.0343	62.92	0.0121	1292	6.3×10^{-4}
$(1,\infty)$	0.01	0.8250	5.178	0.1234	69.96	0.0437	1276.	...	...	3.6×10^{-3}
	1.	0.8275	5.267	0.1180	69.67	0.0445	908.5	...	...	2.7×10^{-3}
	5.	0.8925	7.233	0.0782	213.3	0.0263	3096	...	...	7.4×10^{-3}
	10.	0.9405	10.99	0.0524	985.7	...	...	...	...	2.3×10^{-2}
$(10,\infty)$	0.01	0.9360	1.534	0.0413	35.54	0.0200	614.8	...	...	2.6×10^{-3}
	1.	0.9350	1.552	0.0385	32.88	0.0184	288.1	0.0071	4552	7.5×10^{-4}
	5.	0.9620	1.807	0.0348	25.87	...	...	...	...	1.4×10^{-2}
	10.	0.9894	2.313	...	...	...	...	...	...	1.8×10^{-2}
Discharging:										
$(1,\infty)$	5.	−0.6138	5.301	−0.2523	74.83	−0.1061	915.9	...	...	3.3×10^{-3}
$(10,\infty)$	5.	−0.8115	1.595	−0.0921	10.94	−0.0656	128.9	−0.0241	2769	2.8×10^{-3}

ier-transform technique and determines, by statistical tests, the most probable value of N_α. The coefficients, exponents, and standard deviation σ of the fit are given in Table II. Although the system response is not strictly a sum of exponentials, the exponential fit provides a convenient means of summarizing the results. In most cased, a fit with $\sigma < 5 \times 10^{-3}$ was achieved with three or four exponentials, and comparisons of the fits for different V_a^* reveals clearly perceptible trends in the coefficients and exponents.

Two simulations were done for $M = 20$ and are included in Table II. As can be seen from Table II, the coefficients and exponents [Eq. (76)] determined for the current-time curves are quite similar to those in the corresponding $M = 10$ simulations. The current-time curves for $M = 20$ would have overlapped those for $M = 10$ had they been included in Fig. 3. Since, in these $M = 20$ simulations, the concentration of the charge carriers in the central 20 Debye lengths of the system ($l = 40 L_D$) was only slightly perturbed by the applied potential difference, it seemed that the system could alternatively be modeled as an $M = 10$ system in series with a parallel RC section whose resistance and capacitance equalled those of the central 20 Debye lengths of the $M = 20$ system. A simulation was completed for this circuit with $V_a^* = 5$, using the approach described in Sec. IV [see Eq. (75)]. The resulting current-time curves agreed to well within 1% with those obtained in the standard simulation, suggesting that such an approach may be useful in treating even larger systems.

The response of a system with blocking electrodes to an applied step-function potential difference has not been treated extensively in the past. The problem has been approached by Jaffé[18,40] using approximate analytic methods and by Kahn and Maycock[10] using numerical techniques. Jaffé made the assumption that the electric field remains uniform throughout the material and predicted that at early times the decay of the total current would be exponential with a decay constant (α/M) proportional to $(V_a^*)^2 M^{-2}$. The constant field approximation is reasonable for thin systems, $M \ll 1$, but wholly inappropriate in the more usual $M \gg 1$ case. Our results for $M = 1$ show a marked increase in the principal decay constant (the α_i in Table II which corresponds to the largest c_i) over the range $0.01 \leqslant V_a^* \leqslant 10$ but not a $(V_a^*)^2$ dependence.

The work of Kahn and Maycock[10] differs from ours in that much larger systems are treated and an explicit finite-difference method with a uniform spatial mesh ($N_\Delta \sim 800$) is used. Kahn and Maycock were somewhat limited by their choice of method and size of the system, and most of their published results are reported for $T \leqslant M$ and $V_a^* \leqslant 2$. The method employed in the present work is, in principle, more powerful than that used by these authors but has not yet been extensively applied to systems of comparable size. From an approximate exponential analysis of their current-time curves, Kahn and Maycock concluded that the dominant exponential decay constant was independent of V_a^* and proportional to M^{-1}. We find that the principal decay constant varies somewhat with V_a^* for $M = 10$ and 20, but not as much as in the $M = 1$ case. The exponents α_i [Eq. (76)] in our notation are M times larger than the decay constants of Kahn and Maycock. Thus, the similarity in the entries in Table II for $M = 20$ and the corresponding $M = 10$ cases is in accord with the observation of those authors for larger systems.

It is instructive also to consider briefly the exact solution of the small-signal case. Although the exact small-signal impedance is known for the model considered here,[1] it has a rather complicated form. In the low-frequency limit, however, there is a simple equivalent circuit for the completely blocking system[1,22,41] which is characterized by a single RC time constant. It follows that at long times, $T > M$, the system response to a small step-function perturbation ($V_a^* \ll 1$) should be governed by this time constant. We find good agreement between the small-signal result (e.g., the small signal $\alpha \approx 2.68$ for $M = 1$, $\pi_m = 1$) and α_1 in Table II for $\pi_m = 1$ and ∞ with $V_a^* = 0.01$, but poor agreement in the $\pi_m = 5$ case, perhaps reflecting the somewhat arbitrary nature of a multiexponential representation for a decay which is not a true sum of exponentials.

An important consequence of the nonlinearity of Eqs. (63)–(65) is that the current-vs-time behavior which follows the application of a step-function potential difference to the originally flatband system is not duplicated when the potential difference between the electrodes is abruptly reduced to zero (i.e., an external short is applied). In Fig. 6, we compare, for the one-mobile $\pi_m = \infty$ case, the current-vs-time behavior following the application of a near step function $V_a^* = 5$

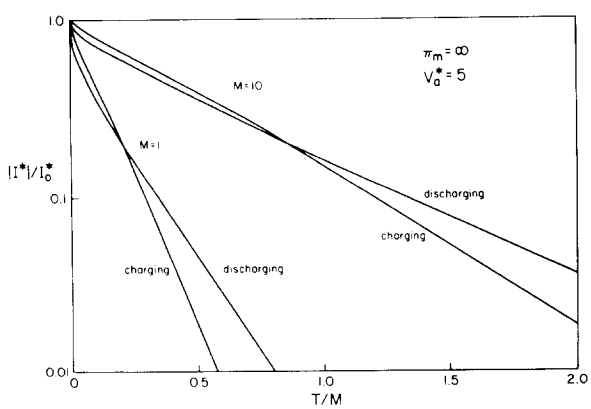

FIG. 6. Current-time curves for charging and discharging of systems with a mobility ratio $\pi_m = \infty$.

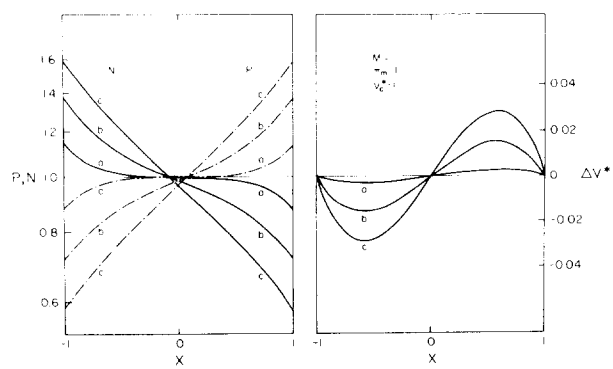

FIG. 7. Stages in the transient response of an $M = 1$, $\pi_m = 1$ system to step function $V_a^* = 1$. (a) $T = 0.061$, (b) $T = 0.32$, (c) $T = \infty$. ΔV^* defined in Eq. (77).

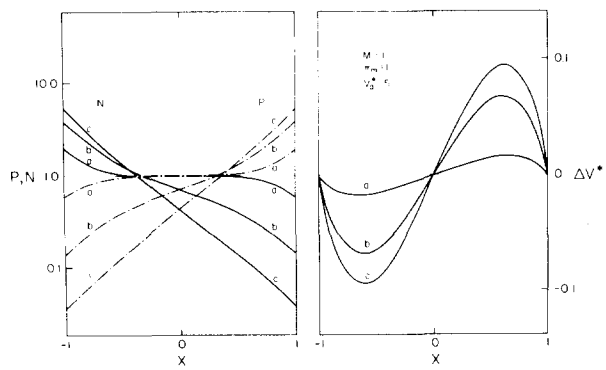

FIG. 8. Stages in the transient response of an $M=1$, $\pi_m=1$ system to step function $V_a^*=5$. (a) $T=0.068$, (b) $T=0.33$, (c) $T=\infty$.

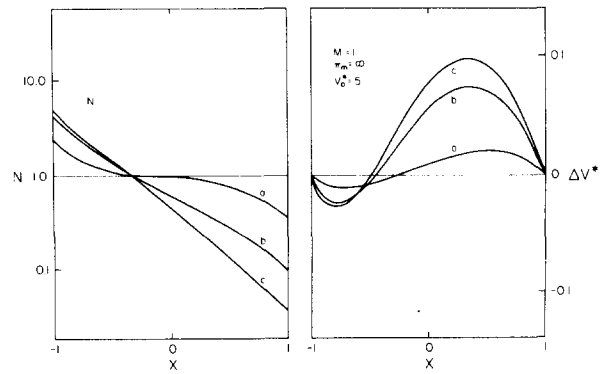

FIG. 10. Stages in the transient response of an $M=1$, $\pi_m=\infty$ system to step function $V_a^*=5$. (a) $T=0.057$, (b) $T=0.23$, (c) $T=\infty$.

(charging) with that following the removal of the applied potential difference in the same near-step-function manner (discharging). It is reasonable that the discharging current is greater in magnitude than the charging current for $T \gtrsim M$, since the concentration of the mobile species in the largest part of the system is increasing with time in the discharging case but decreasing in the charging situation. The charging and discharging curves must cross if the total quantity of charge transported in each case is to be the same. The discharging curves were also fitted to a sum of exponential decays [Eq. (76)], and the resulting coefficients and exponents have been included in Table II.

Figures 7–13 show the development in time of the space-charge layers and the potential distribution in the system. For the $M=1$ systems, the potential is shown as

$$\Delta V^* \equiv V^* - V_{\text{lin}}^*, \tag{77}$$

where $V_{\text{lin}}^* \equiv -V_a^* X/2M$ is the linear potential which falls across the system before any movement of the charges occurs. Figure 7 shows N, P, and ΔV^* at three stages in the evolution of an $M=1$, $\pi_m=1$ system with $V_a^*=1$. Figure 8 shows the same quantities at nearly the same times for $M=1$, $\pi_m=1$, and $V_a^*=5$. Perhaps the most striking difference between these two cases is the far greater depletion of charge carriers in the center of the system for $V_a^*=5$. This depletion becomes even more pronounced as V_a^* is increased. Figures 8–10 show the role of the mobility ratio in the response of an $M=1$ system to a $V_a^*=5$ applied potiential step. In the $\pi_m=1$ case, there is symmetry about the center of the system, with $N(X)=P(-X)$ and $V(X)=-V(-X)$. In the $\pi_m=5$ case (Fig. 9), one finds that the more mobile negative carriers assume a near-steady-state distribution well in advance of the slower positive carriers. The charge and potential distributions are asymmetric in this case until the final mobility-independent symmetric equilibrium state is established. Figure 10 displays the response of a strictly one-mobile system, $\pi_m=\infty$, for which the final state is asymmetric. It should be noted that in all the $M=1$ cases (as in thin films and membranes) the deviation of the final state potential distribution from linearity is only a few percent of V_a^*. Further, in the one-mobile case, the greater part of the potential drop falls across the part of the system which has been depleted of mobile carriers ($N<1$).

Figure 11–13 show stages in the response of three $M=10$ systems with different mobility ratios to a $V_a^*=5$ step-function applied potential difference. For clarity, only the two Debye lengths nearest each electrode are shown. As in the $M=1$ cases discussed above, the response of the $\pi_m=1$ system (Fig. 10) is characteristically symmetrical, while only the equilibrium state is symmetrical for $\pi_m=5$. Also, in the $\pi_m=\infty$ case, the major portion of the potential drop falls across the depletion region, as was the case for $M=1$. The response of $M=10$ systems for $V^*=1$ and 10 (not shown) shows considerable qualitative similarity to that for $V^*=5$.

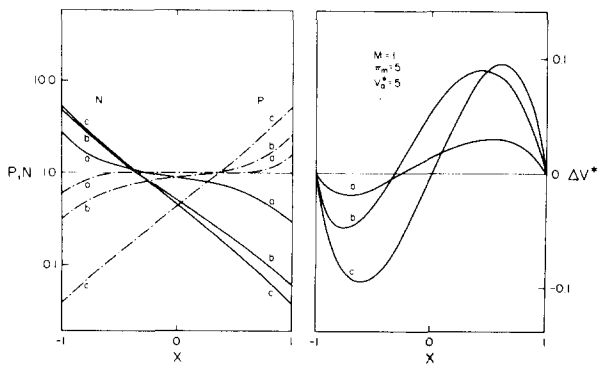

FIG. 9.Stages in the transient response of an $M=1$, $\pi_m=5$ system to step function $V_a^*=5$. (a) $T=0.092$, (b) $T=0.41$, (c) $T=\infty$.

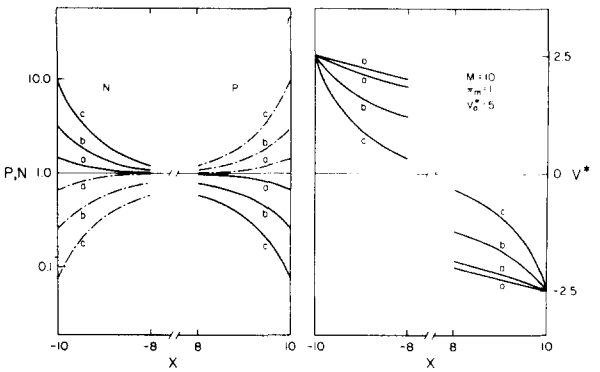

FIG. 11. Stages in the transient response of an $M=10$, π_m system to step function $V_a^*=5$. Only the two Debye lengths nearest each electrode are shown. (0) $T=0$, (a) $T=1.2$, (b) $T=6.3$, (c) $T=\infty$.

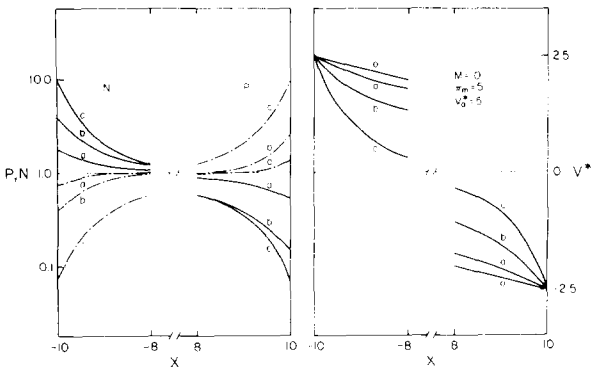

FIG. 12. Stages in the transient response of an $M=10$, $\pi_m=5$ system to step function $V_a^*=5$. (0) $T=0$, (a) $T=1.6$, (b) $T=6.9$, (c) $T=\infty$.

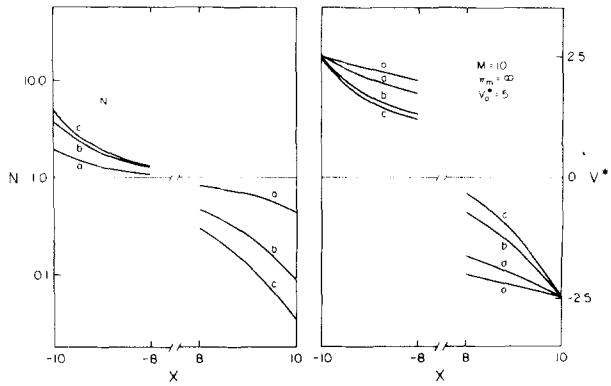

FIG. 13. Stages in the transient response of an $M=10$, $\pi_m=\infty$ system to step function $V_a^*=5$. (0) $T=0$, (a) $T=1.9$, (b) $T=8.0$, (c) $T=\infty$.

For the final equilibrium state, the quantity V^*/V_a^* is, to a fair approximation, independent of V_a^* for $V_a^* \leqslant 10$. (For $V_a^* > 10$, the equilibrium V^*/V_a^* does show a dependence on V_a^*, reflecting depletion of charge carriers from the center of the system.) The time dependence of the system response does, however, vary considerably over the range $1 \leqslant V_a^* \leqslant 10$ (recall Figs. 3–5). Although the P-, N-, and V^*-vs-X curves have the same qualitative time dependence throughout this range, the time required for a given fraction of the space-charge layer to accumulate at the electrodes increases several fold from $V_a^*=1$ to 10.

VI. SUMMARY

The steady-state and transient response of a material containing one or two species of mobile charge carriers which are completely blocked at the electrodes have been investigated. The steady-state charge and potential distributions for illustrative cases have been included in Figs. 8–13, and the static capacitance of a number of systems was shown in Figs. 1 and 2 as a function of the applied potential drop.

The transient response of systems to a near-step-function applied potential difference was simulated with the aid of POST, a sophisticated package of FORTRAN subroutines for the solution of coupled partial and ordinary differential equations. The simulation results show clearly the role of system length and the charge carrier mobility ratios in determining system response. We intend, in future work, to allow for extrinsic conduction, charge carrier reactions at the electrode and in the bulk of the material, intrinsic space-charge layers, and elementary discreteness of charge and compact layer effects, as has already been done in the exact treatment of the small-signal case. Although computational expense remains a limiting factor in work of this sort, we believe that existing numerical techniques can provide a useful approach to the study of systems of a realistic degree of complexity and will aid greatly in the interpretation of large-signal electrical response.

ACKNOWLEDGMENTS

We are grateful to Dr. N.L. Schryer, author of the POST program, for appreciable aid in its implementation and to T.R. Brumleve for a number of helpful discussions.

[1] J.R. Macdonald and D.R. Franceschetti, J. Chem. Phys. **68**, 1614 (1978).
[2] D.R. Franceschetti, J. Appl. Phys. **48**, 3439 (1977).
[3] D.R. Franceschetti, and J.R. Macdonald, J. Electroanal. Chem. **82**, 271 (1977).
[4] J. Frenkel, *Kinetic Theory of Liquids* (Oxford U.P., New York, 1946), p. 36.
[5] J.R. Macdonald, Solid-State Electron. **5**, 11 (1962).
[6] H.K. Gummel, IEEE Trans. Electron Devices **ED-11**, 455 (1964).
[7] A. De Mari, Solid-State Electron. **11**, 1021 (1968).
[8] M. Kurata, IEEE Trans. Electron Devices **ED-19**, 1207 (1972).
[9] C.M. Lee, R.J. Lomax, and G.I. Haddad, IEEE Trans. Microwave Theory **MTT-22**, 160 (1974).
[10] D. Kahn and J.N. Maycock, J. Chem. Phys. **46**, 4434 (1967).
[11] H. Cohen and J.W. Cooley, Biophys. J. **5**, 145 (1965).
[12] S.W. Feldberg, in *Electroanalytical Chemistry*, edited by A.J. Bard (Dekker, New York, 1969), Vol. 3, p. 199.
[13] R. de Levie and H. Moriera, J. Membrane Biol. **9**, 241 (192).
[14] J.R. Sandifer and R.P. Buck, J. Electroanal. Chem. **49**, 161 (1974).
[15] T.R. Brumleve and R.P. Buck, J. Electroanal. Chem. **90**, 1 (1978).
[16] Z. Galus, *Fundamentals of Electrochemical Analysis*, translated by G.F. Reynolds (Halsted, New York, 1976).
[17] B.E. Conway and H. Angerstein-Kozlowska, in *Electrochemistry on Non-Metallic Surfaces* edited by A.D. Franklin, NBS Spec. Pub. 455 (U.S. GPO, Washington, D.C., 1976), p.107.
[18] G. Jaffé, Ann. Phys. **16**, 217 (1933).
[19] J.R. Macdonald, J. Chem. Phys. **29**, 1346 (1958).
[20] J.R. Macdonald, J. Chem. Phys. **30**, 806 (1959).
[21] J.R. Macdonald, J. Appl. Phys. **46**, 4602 (1975).
[22] J.R. Macdonald, J. Chem. Phys. **58**, 4982 (1973).
[23] A. Erdélyi, W. Magnus, F. Oberhettinger, and F.G. Tricomi, *Higher Trancendental Functions* (McGraw-Hill, New York, 1953), Vol. II, p. 294ff.
[24] D.J. Hofsommer and R.P. van de Riet, Num. Math. **5**, 291 (1963).
[25] J.L. Blue, Bell Syst. Tech. J. **56**, 1651 (1977).
[26] P.A. Fox, A.D. Hall, and N.L. Schryer, Bell Laboratories Computing Science Technical Report No. 47, 1976 (unpublished).
[27] J.R. Macdonald, J. Chem. Phys. **22**, 1317 (1954).
[28] B. Carnahan, H.A. Luther, and J.O. Wilkes, *Applied Numerical Methods* (Wiley, New York, 1969), p. 429ff.
[29] J.H. Kohl and D.J. Hamilton, J. Electrochem. Soc. **124**, 1912 (1977).
[30] L.C. McAfee, Jr., IEEE Trans. Electron Devices **ED-23**, 442 (1976).
[31] L.C. McAfee, Jr., IEEE Trans. Electron Devices **ED-23**, 447 (1976).
[32] D.H. Norie and G. DeVries, *The Finite Element Method* (Academic, New York, 1973).
[33] M.E. Gurtin, Q. Appl. Math. **22**, 252 (1964).
[34] N.L. Schryer, Bell Laboratories Computing Science Technical Report No. 53, 1977 (unpublished).
[35] N.L. Schryer, Bell Laboratories Computing Science Technical Report No. 52, 1976 (unpublished).
[36] C. de Boor, J. Approx. Theory **6**, 50 (1972).
[37] N.L. Schryer (private communication).
[38] S.W. Provencher, Biophys. J. **16**, 27 (1976).
[39] S.W. Provencher, J. Chem. Phys. **64**, 2772 (1976).
[40] G. Jaffé, Ann. Phys. **16**, 249 (1933).
[41] J.R. Macdonald, J. Electroanal. Chem. **53**, 1 (1974).